Journal of Physiology (1992), **457**, *pp.* 591–610
With 13 *figures*
Printed in Great Britain

VOLTAGE-DEPENDENT IONIC CURRENTS IN DISSOCIATED PARATRACHEAL GANGLION CELLS OF THE RAT

BY KEIJI AIBARA, SATORU EBIHARA AND NORIO AKAIKE

From the Department of Neurophysiology, Tohoku University School of Medicine, Sendai 980, Japan

(*Received 3 October 1991*)

SUMMARY

1. Conventional whole-cell voltage-clamp technique was used to study the electrophysiological and pharmacological properties of voltage-dependent Na^+, K^+ and Ca^{2+} channels in parasympathetic neurones enzymatically dissociated from the paratracheal ganglia of rat trachea. The voltage-dependent Na^+, K^+ and Ca^{2+} currents (I_{Na}, I_K and I_{Ca}) were separated by the use of ion subtraction and pharmacological treatments.

2. I_{Na} was activated by a step depolarization more positive than -50 mV and fully activated at positive potentials more than $+10$ mV. The inactivation phase of I_{Na} consisted of fast and slow exponential components (τ_{if} and τ_{is}, respectively). The τ_{if} and τ_{is} were voltage dependent and decreased with a more positive step pulse.

3. The time course for recovery of I_{Na} from the complete inactivation exhibited two exponential processes.

4. The reversal potential of I_{Na} was equal to the Na^+ equilibrium potential (E_{Na}) and resembled a simple Na^+ electrode depending only on external Na^+ concentration.

5. Tetrodotoxin (TTX) reduced I_{Na} without affecting the current kinetics in a concentration-dependent manner, and the concentration of half-maximal inhibition (IC_{50}) was 6×10^{-9} M. There was no TTX-resistant component of I_{Na} in any of the cells tested.

6. Scorpion toxin increased the peak amplitude of I_{Na} and prolonged the inactivation phase in a time- and concentration-dependent manner. In the presence of toxin, both τ_{is} and the fractional contribution of the slow current component to total I_{Na} increased concentration dependently.

7. High-threshold (L-type) I_{Ca} was activated by a step depolarization more positive than -30 mV and reached a peak at near 0 mV in the external solution with 2·5 mM Ca^{2+}. The current was inactivated to only a small extent ($< 10\%$) during 100 ms of depolarizing step pulse. There was no low-threshold (T-type) I_{Ca} in this preparation.

8. The maximum I_{Ca} in individual current–voltage (I–V) relationships was saturated by an increase in extracellular Ca^{2+} concentration ($[Ca^{2+}]_o$). The I–V relationships were also shifted along the voltage axis to the more positive potential with increasing $[Ca^{2+}]_o$.

MS 9787

9. The inactivation process of the L-type I_{Ca} was dependent on Ca^{2+} influxes (I_{Ca}-dependent inactivation).

10. Relative maximum peak currents of divalent cations passing through the L-type Ca^{2+} channels were in the order of $I_{Ba} > I_{Ca} > I_{Sr}$.

11. Organic and inorganic Ca^{2+} antagonists blocked the I_{Ca} in a concentration-dependent manner. The order of inhibition was ω-conotoxin > flunarizine > nimodipine > D600 > diltiazem $\gg$ amiloride for organic blockers and $La^{3+} > Cd^{2+} > Ni^{2+} > Co^{2+}$ for inorganic ones.

12. Three types of I_K were observed; i.e. an inwardly rectifying current, a delayed outward current (I_{KD}), and a transient outward current (I_A).

13. Depolarizing pulses from a holding potential (V_H) of -90 mV elicited K^+ currents which seemed to suggest the existence of two distinct cell types. The I_A was observed in the majority of cells (44 out of 63 cells). The I_{KD} was elicited in all cells tested.

14. I_{KD} was activated by step pulses more positive than -20 mV, slowly inactivated ($\tau > 1$ s) and reduced by adding tetraethylammonium (IC_{50} was 4·4 mM).

15. The I_A was characterized by a rapid activation and inactivation. The amplitude of I_A was reduced by 4-aminopyridine (IC_{50} was about 4·3 mM) but the current was not affected by the removal of $[Ca^{2+}]_o$.

INTRODUCTION

Since voltage-clamp analysis of neuronal membrane currents has been applied to various neurones from both central nervous system and peripheral ganglia, the information about the roles of various membrane conductances responsible for neuronal excitability has greatly increased (for review, see Kostyuk, 1984; Adams & Galvan, 1986). One class of vertebrate neurones whose electrophysiological properties have received relatively little attention is the paratracheal neurones. The neurones are organized into ganglia that are concentrated along the posterior wall of the trachea (Honjin, 1954; Fisher, 1964). Because of the relative inaccessibility and small size of these ganglia, the electrophysiological approach to the neurones was difficult. In the last, decade, however, some approaches by the use of conventional glass microelectrodes have been made on the paratracheal neurones *in situ* of the ferret, cat and rabbit (for review, see Coburn, 1987) and also the cultured paratracheal neurones of the rat (Burnstock, Allen & Hassall, 1987) in current-clamp condition. Voltage-clamp study also has been applied to the rat paratracheal cells (Allen & Burnstock, 1990*a*, *b*). However, a systematic description of the membrane conductances in these cells has not been reported.

Recently, we successfully dissociated single neurones from the paratracheal ganglia of rat trachea. The dissociated neurones were more suitable for voltage-clamp experiments, and we have investigated the property of acetylcholine-activated ionic currents using this preparation (Aibara & Akaike, 1991). In the present study, we have investigated physiological and pharmacological characteristics of the voltage-dependent ionic currents in dissociated rat paratracheal neurones using the conventional whole-cell patch-clamp technique.

METHODS

Dissociation of paratracheal neurones

The experiments were performed on single paratracheal neurones freshly dissociated from 1- to 2-week-old Wistar rats. The procedure for obtaining dissociated paratracheal ganglion cells is similar to that described elsewhere (Aibara & Akaike, 1991). Briefly, a membranous portion

TABLE 1. Composition of solutions used (mM)

External solutions	NMG-Cl	NaCl	KCl	CsCl	$CaCl_2$	$MgCl_2$	glucose	HEPES
E_1	60	90	—	5	2	1	10	10
E_2	140	—	—	5	10	1	10	10
E_3	150	—	5	—	2	1	10	10
Internal solutions	**NMG-Cl**	**NaCl**	**KCl**	**CsCl**	**TEA-Cl**	**MgATP**	**EGTA**	**HEPES**
I_1	90	30	—	—	20	2	10	10
I_2	90	—	—	30	20	2	10	10
I_3	20	—	120	—	—	2	10	10

All external and internal test solutions were adjusted to pH 7·4 and 7·2 with Tris-base, respectively. Solutions E_1 and E_3 contained 0·5 mM $CdCl_2$ to block Ca^{2+} currents. Solutions E_2 and E_3 contained 3 μM TTX to block Na^+ currents. Solutions I_2 additionally contained 0·2 mM Na_2GTP and 0·5 mM cyclic AMP. NMG-Cl, *N*-methyl-D-glucamine chloride.

containing paratracheal ganglia was rapidly removed from the trachea of rats under ether anaesthesia, and the ganglia were treated with 0·2% trypsin for 20–30 min at 37 °C and subsequently with a solution containing 0·3% collagenase for 20–30 min. Thereafter, the ganglion cells were dissociated mechanically by gentle pipetting of the membranous portion in a culture dish, and the dissociated cells adhered to the bottom of the dish within 30 min. Then, the cells were prepared for the electrophysiological experiments. All experiments were carried out at room temperature (20–22 °C).

Solutions and chemicals

The composition of test solutions, unless otherwise noted, is summarized in Table 1. Drugs and toxins used in the present experiment were scorpion venom from *Leiurus quinquestriatus*, tetrodotoxin and amiloride (Sigma), ω-conotoxin (Peptide), flunarizine (Kyowa Hakko), D600 (Knoll), diltiazem (Tanabe), nimodipine (Bayer), *N*-methyl-D-glucamine chloride (NMG-Cl), tetraethylammonium chloride (TEA-Cl) and 4-aminopyridine (4-AP; Tokyo Kasei).

The external test solution was exchanged by a rapid application technique termed the 'Y-tube' method, which causes the solution surrounding a dissociated neurone to change completely within 10–20 ms (Akaike, Shirasaki & Yakushiji, 1991).

Electrophysiological measurements

The voltage-dependent Na^+, K^+ and Ca^{2+} currents in dissociated paratracheal ganglion cells were recorded in the whole-cell configuration by the use of a conventional patch-clamp technique (Hamill, Marty, Neher, Sakmann & Sigworth, 1981). Patch pipettes were made using borosilicate glass capillary tubes (1·5 mm o.d.; Narishige) and a vertical puller (PB-7; Narishige). When the patch electrodes were filled with internal solutions, the resistance was in the range of 4–10 MΩ. When the pipettes were placed in the external solution, the junction potential was compensated with an off-set circuit in the amplifier (L/M-EPC7; List-Medical). Series resistance and cell membrane capacitance were estimated from the transient compensation dial settings on the amplifier after optimum reduction of the capacitative transient. During voltage-clamp experiments 50–90% of the series resistance was electronically compensated.

The membrane current and potential were monitored on a storage oscilloscope (MS-5100A; Iwatsu) after low-pass filtering at 10 kHz (2-pole Bessel) in the amplifier, and were simultaneously recorded in video cassette recorder (HV-F73; Mitsubishi) with a pulse code modulator (PCM-

501ES; Sony). The recorded data were digitalized (sampling time interval of 50 μs; 12-bit resolution) using a microcomputer (IBM AT compatible) and stored on a floppy disk. The stored data were further analysed on the microcomputer using the P-CLAMP program (version 5·5; Axon Instruments). Periods of 400–500 μs at the onset of the command pulses have been removed from all current records to remove spurious points due to incomplete capacitive compensation. In some experiments, the current recordings were not corrected for leakage and capacitative currents. However, in those cases where corrections were made, TTX and Cd^{2+} were used to block Na^+ and Ca^{2+} currents, respectively. The 'net' Na^+ and Ca^{2+} currents were taken as TTX- and Cd^{2+}-sensitive currents, respectively. Averaged values are shown as means ± S.E.M.

RESULTS

The average resting membrane potential of dissociated paratracheal ganglion cells measured immediately after the destruction of patch membrane was $-51{\cdot}9 \pm 1{\cdot}1$ mV (range: -43 to -65 mV, $n = 104$). The value was close to the average value of $-57{\cdot}1$ mV recorded from the paratracheal neurones *in situ*, using a glass microelectrode, by Allen & Burnstock (1990*a*). The following physiological and pharmacological studies were made on the voltage-dependent Na^+, Ca^{2+} and K^+ currents (I_{Na}, I_{Ca} and I_K, respectively) of paratracheal ganglion cells, in which each current was separated from others by the use of ion substitution and pharmacological treatments.

Sodium current (I_{Na})

When I_{Na} was recorded in external test solution containing 150 mM Na^+ at a holding potential (V_H) of -100 mV, the inward currents appeared abruptly at small depolarizing voltage pulses, indicating the failure of the space clamp (Fig. 1*B*). Thus, voltage-dependent I_{Na} was recorded from the neurones perfused with internal (I_1) and external (E_1) solutions containing 30 and 90 mM Na^+, respectively (see Table 1). In this experimental condition, we could record reasonable current–voltage (*I–V*) relationships of I_{Na} (see Fig. 1*B*). Therefore, I_{Na} was recorded in the external E_1 solution with 90 mM Na^+, unless otherwise stated. The 'net' I_{Na} was obtained by subtracting currents before and after adding 3 μM tetrodotoxin (TTX) to the external solution, at which concentration TTX completely suppressed I_{Na} (Kaneda, Oyama, Ikemoto & Akaike, 1989*a*). An example of 'net' I_{Na} recorded from the same cell is shown in Fig. 1*A*. The current was rapidly activated, reached peak amplitude, and then displayed a rapid inactivation. Figure 1*B* shows the *I–V* relationships for I_{Na} recorded from the same neurone in the external test solutions containing four different Na^+ concentrations (30, 50, 90 and 150 mM). The V_H was -100 mV. The threshold for detectable I_{Na} was -50 mV and the maximum I_{Na} appeared in the potential range of -20 to -10 mV. When the intracellular Na^+ concentration ($[Na^+]_i$) was 30 mM, the peak amplitude and the reversal potential of I_{Na} were dependent on the external Na^+ concentration ($[Na^+]_o$). Figure 1*C* shows the mean reversal potential of I_{Na} plotted as a function of the logarithm of $[Na^+]_o$ activity. The data points were close to a straight line which shows the change of the Na^+ equilibrium potential (E_{Na}).

Figure 2*A* shows a relationship between voltage and peak Na^+ conductance calculated from the chord conductance equation:

$$g_{Na} = I_{Na}/(V - E_{Na}), \quad (1)$$

where g_{Na} is peak Na^+ conductance at potential V, I_{Na} is peak current, and E_{Na} is the Na^+ equilibrium potential. The continuous line is a least-squares fit to a Boltzmann function:

$$g/g_{max} = 1/[1+\exp((V-V_{0.5})/k)], \quad (2)$$

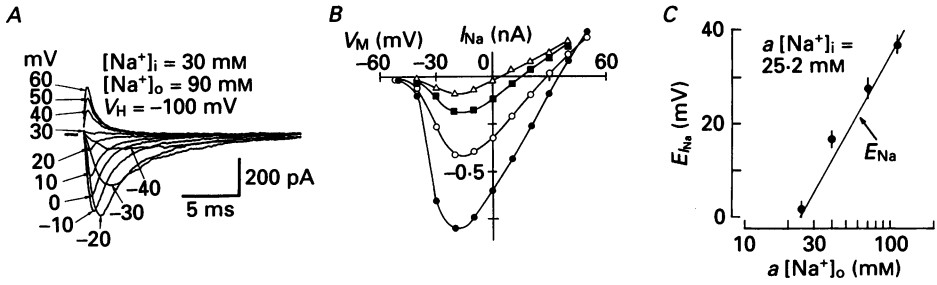

Fig. 1. Membrane properties of the voltage-dependent Na^+ currents (I_{Na}). *A*, a typical example of I_{Na} from the same neurone at a V_H of -100 mV. Depolarizing command voltages are -40, -30, -20, -10, 0, $+10$, $+20$, $+30$, $+40$, $+50$ and $+60$ mV. The currents were corrected for leakage and capacity currents after blocking I_{Na} by adding 3 μM TTX. *B*, current–voltage (I–V) relationships for peak I_{Na} recorded in the external test solutions containing Na^+ of the following concentrations (mM): △, 30; ■, 50; ○, 90; ●, 150. The internal solution contained 30 mM Na^+. The data were obtained from the same neurone at a V_H of -100 mV. V_M, membrane potential. *C*, relationship between the reversal potential of peak I_{Na} ($E_{I_{Na}}$) and external Na^+ activity ($a[Na^+]_o$). The Na^+ activity was measured by G502 Na sodium electrode connected to an ION 85 ion analyser (A/S; Radiometer). Each point is the mean from five to seven neurones. Vertical bars indicate the mean ± S.E.M. A straight line shows the theoretical change of the Na^+ equilibrium potential (E_{Na}).

where g/g_{max} is the fractional membrane conductance, V is a membrane potential, $V_{0.5}$ is half-activation potential, and k is a slope factor. Figure 2*A* shows that the Na^+ conductance activates over the potential range of -50 to $+10$ mV; mean values of $V_{0.5}$ and k are $-20 \pm 3{\cdot}7$ mV ($n = 5$) and $-7{\cdot}3 \pm 0{\cdot}4$ mV ($n = 5$), respectively.

Steady-state inactivation (h_∞) of I_{Na} was studied using the conventional double-pulse protocol shown in Fig. 2*B*. A 3 s conditioning prepulse (CP) was applied from a V_H of -100 mV. A 50 ms test pulse (TP) to 0 mV was subsequently applied after an interval of 0·5 ms. The continuous line in the figure represents a theoretical single Boltzmann distribution. The I_{Na} inactivated over the potential range of -120 to -40 mV. The half-inactivated potential was $-74 \pm 3{\cdot}2$ mV ($n = 6$), and the slope factor was $8{\cdot}3 \pm 0{\cdot}3$ mV ($n = 6$). If the inactivation is well represented by a single exponential process, a semilogarithmic plot of $(1\text{-}h_\infty)/h_\infty$ against prepulse potential should yield a straight line. Our data points deviated a little from linearity at potentials more negative than -90 mV. However, this deviation was not statistically significant (not shown).

The activation kinetics of I_{Na} was clearly dependent on depolarizing test potentials, as shown in Fig. 1*A*. The activation time (time to peak) decreased much more with greater positive potentials. However, the detailed analysis of the activation kinetics was impossible because of the interference of transient capacitative current on I_{Na}. On the other hand, the inactivation kinetics could be clearly analysed by using either

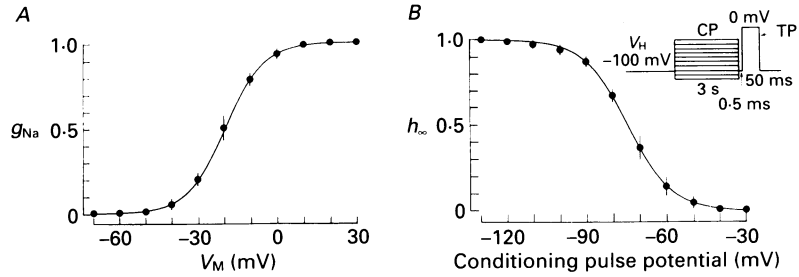

Fig. 2. Activation and inactivation kinetics of I_{Na}. *A*, conductance–voltage relationship for peak I_{Na}. Chord conductance (g_{Na}) was calculated from eqn (1) (see text). The normalized conductance is plotted as a function of membrane potential. The plot shows the best fit of eqn (2) to data (see text). The best-fit line had $V_{0·5} = -20$ mV and $k = -7·3$ mV (see text for explanation of symbols). Data points are the average of five neurones and the vertical bars indicate ± S.E.M. *B*, steady-state inactivation (h_∞) curve of I_{Na}. The pulse protocol is shown in the inset. The $h_{0·5}$ was −74 mV. A line drawn through the data points represents a theoretical single Boltzmann distribution. Each point is the mean from six neurones.

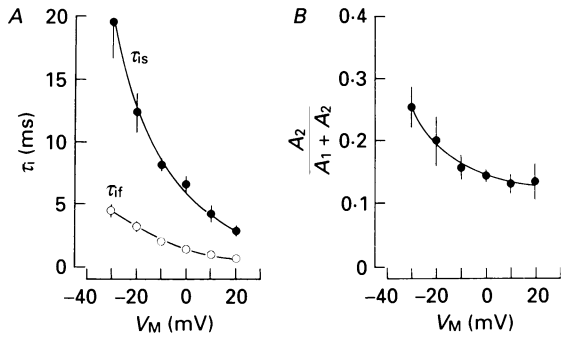

Fig. 3. Time course of inactivation process of I_{Na}. *A*, mean fast and slow time constants (τ_{if} and τ_{is}) of I_{Na} inactivation plotted as a function of membrane potential (V_M). I_{Na} was elicited by the depolarizing test pulses from a V_H of −100 mV. Time constants were determined by using an exponential curve fitting program. The inactivation phase of I_{Na} was fitted by an equation describing the sum of two exponentials: $A_1 \exp(-T/\tau_1) + A_2 \exp(-T/\tau_2) + A_0$, where A_1, A_2 and A_0 are the amplitudes of the fast and slow time constants and steady-state component, respectively ($\tau_1 < \tau_2$), and T is time (Follmer *et al.* 1987). *B*, contribution of the fast (A_1 and the slow (A_2) time constants to the inactivation depends on the membrane potential. A line through data points was drawn by eye. Data points are means ± S.E.M. ($n = 5$–7).

the exponential curve fitting of individual currents or a double-pulse protocol. The time course of I_{Na} inactivation was determined from the decay phase of I_{Na} which was fitted to the sum of two exponentials using a computerized curve-fitting program. Both the fast and slow time constants (τ_{if} and τ_{is}, respectively) had voltage dependence, and they decreased as test potentials became more positive (Fig. 3*A*). The mean value of τ_{if} is more than four times less than that of τ_{is}. The contribution of the slow current component to total inactivation decreased with more positive potentials in a potential-dependent manner (Fig. 3*B*).

The I_{Na} inactivation was studied by using double-pulse protocol. The prepulses having various durations and amplitudes were applied from a V_H of −100 mV, and

a 50 ms test pulse was subsequently applied to 0 mV after an interval of 0·5 ms. Inactivation of I_{Na} was dependent on both the duration and amplitude of the prepulse (Fig. 4*A*, upper panel). In the lower panel of Fig. 4*A*, the inactivation process of I_{Na} plotted on a semilogarithmic scale showed that all inactivation time

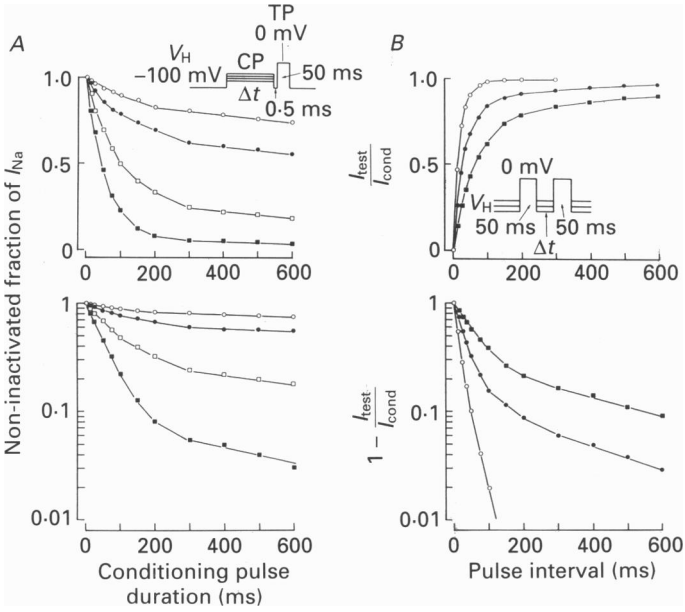

Fig. 4. Inactivation and reactivation of I_{Na}. *A*, time course of inactivation of I_{Na}. The pulse protocol is shown in the inset: pulse applied at 0·1 Hz. Voltage steps to: ○, −80; ●, −70; □, −60; ■, −50 mV. In the upper panel, peak current is plotted as the non-inactivated fraction of I_{Na} against conditioning pulse duration (same symbols as in lower panel). In the lower panel, data plotted on a semilogarithmic scale to show the presence of at least two time constants in the inactivating process. *B*, time course of reactivation of I_{Na} at three different V_H: ○, −100; ●, −90; ■, −70 mV. The pulse protocol is shown in the inset. I_{cond} and I_{test} show I_{Na} during conditioning pulse and test pulse, respectively. In upper panel, normalized data are plotted as a function of the pulse interval (Δt). Recovery was accelerated by more negative V_H. In lower panel, data are plotted on a semilogarithmic scale to show the presence of more than one exponential recovery process (same symbols as in upper panel).

courses were not well described by a single exponential process, implying the presence of at least two time constants in the inactivating process of I_{Na}.

Figure 4*B* shows the time course of recovery from the complete inactivation of I_{Na}. A pair of 50 ms test pulses to 0 mV was applied from the V_H of three different potentials (−100, −90 and −70 mV). The ratio of peak I_{Na} elicited during the second pulse was plotted against the interval duration (Δt) between the pair pulses (Fig. 4*B*, upper panel). The recovery from inactivation was dependent on the interval duration between the pair pulses, and was accelerated by hyperpolarization of the membrane potential. When the recovery time course of peak I_{Na} was plotted on a semilogarithmic scale, the data points at all V_H clearly deviated from a straight line, indicating the presence of at least two exponential recovery processes (Fig. 4*B*, lower panel).

The effect of TTX was examined on I_{Na} elicited by a 50 ms test pulse to 0 mV from a V_H of -100 mV. Figure 5*Aa* shows that I_{Na} was inhibited in a concentration-dependent manner by adding TTX. The activation and inactivation kinetics of I_{Na} were not affected by TTX. TTX also did not shift the *I–V* relationship of I_{Na}. The

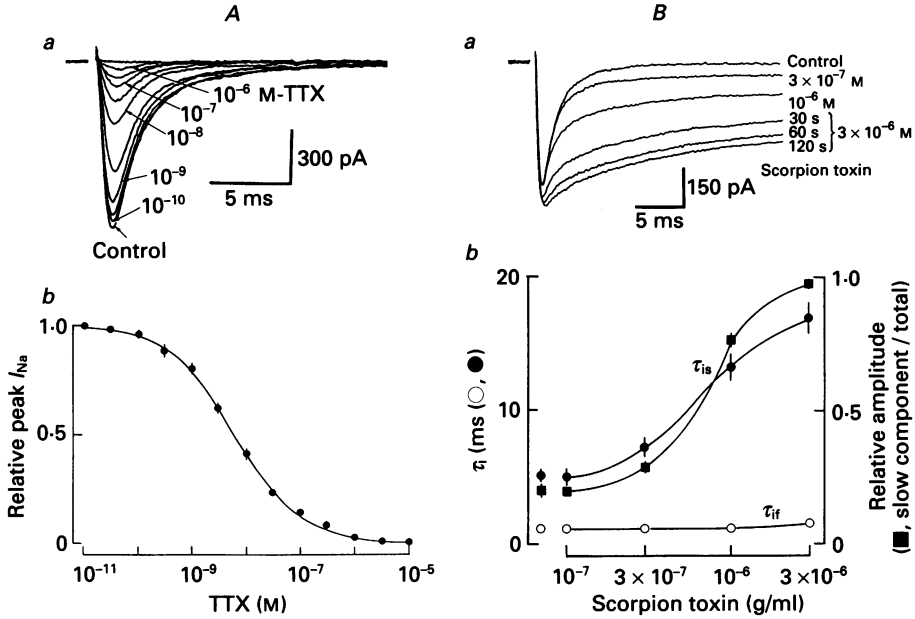

Fig. 5. Effects of tetrodotoxin and scorpion toxin on I_{Na}. *Aa*, an example of I_{Na} from the same neurone in the absence and presence of TTX of various concentrations from 10^{-10}–10^{-6} M. I_{Na} was elicited by depolarized pulse to 0 mV from a V_H of -100 mV. *Ab*, concentration–inhibition curve of TTX for blocking I_{Na}. Normalized peak current amplitudes are plotted as a function of TTX concentration. Data points are means ± S.E.M. ($n = 4$–6). The curve through the data points is fitted by the equation: $I_{Na}/I_{Na,max} = 1/(1+[TTX]/K_d)$, where I_{Na} and $I_{Na,max}$ are the peak amplitudes of I_{Na} in the presence and absence of TTX, respectively. K_d is the dissociation constant ($6{\cdot}1 \times 10^{-9}$ M). [TTX] shows TTX concentration. *Ba*, a typical example of I_{Na} from the same cell in the absence and presence of scorpion toxin of three different concentrations. I_{Na} was elicited by the test pulse to 0 mV from a V_H of -100 mV. *Bb*, concentration-dependent changes of τ_{if} (○) and τ_{is} (●) in the inactivation process of I_{Na}. The symbol (■) shows the fractional contribution of the slow component in the inactivation phase to total inactivation. The data points are means ± S.E.M. ($n = 4$–5). The symbols (○, ●, ■) at the left end are the control values of τ_{if}, τ_{is} and the fractional contribution of the slow component, respectively. Lines were drawn by eye.

threshold concentration for TTX depressing I_{Na} was 3×10^{-11} M, and the concentration of half-maximum inhibition (IC_{50}) was $6{\cdot}1 \times 10^{-9}$ M (Fig. 5*Ab*). In all cells used, I_{Na} was completely abolished by TTX at concentrations beyond 3×10^{-6} M, suggesting that the TTX-resistant component of I_{Na} is absent in this preparation.

The effect of scorpion toxin on I_{Na} elicited by a 50 ms test pulse from a V_H of -100 mV to 0 mV was tested. The toxin increased the peak amplitude of I_{Na} and prolonged the inactivation phase in a time- and concentration-dependent manner (Fig. 5*Ba*). In the presence of the toxin, both the time constant (τ_{is}) of the slow

component in the inactivation phase and its fractional contribution to the total current increased in a concentration-dependent manner, while the fractional contribution of the fast current component decreased without changing its time constant (τ_{if}) (Fig. 5*Bb*). Action of the toxin on Na^+ channels in this preparation was essentially similar to those in other preparations (Gonoi, Hille & Catterall, 1984; Benoit & Dubois, 1987; Kaneda, Oyama, Ikemoto & Akaike, 1989*b*).

Calcium current (I_{Ca})

The voltage-dependent Ca^{2+} current (I_{Ca}) was separated by the perfusion of both internal I_2 solution with 10 mM EGTA and external E_2 solution with 10 mM Ca^{2+}, unless otherwise stated (see Table 1). The 'net' I_{Ca} was obtained by subtracting currents before and after the addition of 0·5 mM $CdCl_2$ to the external solution. Figure 6*A* shows the 'net' I_{Ca} at two different V_H; one was around a 'normal' resting potential (−55 mV), and the other was a hyperpolarized potential (−95 mV). The currents were recorded from the same neurone. After I_{Ca} reached the peak amplitude, the currents persisted with only a little inactivation during a continuous depolarizing pulse. There was no significant difference in the maximum current amplitudes in the individual *I–V* relationships of each neurone at two different V_H, in which the relative value of I_{Ca} at a V_H of −95 mV was $1{\cdot}01 \pm 0{\cdot}03$ ($n = 12$, $P > 0{\cdot}05$) of that at a V_H of −55 mV. The half-times to the peak current were $9{\cdot}5 \pm 0{\cdot}65$ and $9{\cdot}6 \pm 0{\cdot}55$ ms at a depolarizing step pulse to +25 mV at V_H of −55 and −95 mV, respectively. No difference was observed between the two values ($n = 12$, $P > 0{\cdot}05$). These results suggest that there is no 'low-voltage-activated' Ca^{2+} channel (Carbone & Lux, 1987) or 'T-type' Ca^{2+} channel (Nowycky, Fox & Tsien, 1985) in this preparation. Figure 6*B* shows two *I–V* relationships for peak I_{Ca} recorded in the external solution containing 2·5 or 10 mM-Ca^{2+}. The data were obtained from the same cell held at a V_H of −100 mV. In the external solution with 2·5 mM Ca^{2+}, the threshold potential for I_{Ca} was in the range of −40 and −30 mV and the maximum current appeared at near 0 mV. Further depolarization decreased the current amplitude. Increase in the $[Ca^{2+}]_o$ increased the peak amplitude of I_{Ca} in a hyperbolic manner and shifted *I–V* relationship to the right. Figure 6*C* summarizes the relationship between the maximum peak I_{Ca} in the individual *I–V* relationships and $[Ca^{2+}]_o$, in which all I_{Ca} values were normalized to the peak I_{Ca} in the external solution with 10 mM-Ca^{2+}. The data points in Fig. 6*C* were well fitted by a theoretical continuous line drawn according to the following equation with $I_{Ca,max} = 1{\cdot}35$ and $K_a = 3{\cdot}4$ mM:

$$I_{Ca} = \frac{I_{Ca,max}}{1 + K_a/[Ca^{2+}]_o}, \tag{3}$$

where I_{Ca} is peak current, $I_{Ca,max}$ is I_{Ca} when all binding sites are occupied by Ca^{2+}, and K_a is an association constant of the Ca^{2+} binding site. This result indicates the existence of saturable binding sites for Ca^{2+} within the Ca^{2+} channel (Yasui & Akaike, 1986; Carbone & Lux, 1987).

To evaluate the degree of Ca^{2+} channel activation in external solution with 10 mM Ca^{2+}, g_{Ca} normalized to maximum g_{Ca} was plotted *versus* the clamp potential (V_C) in Fig. 7*A*. The g_{Ca} corresponded to the peak I_{Ca} evoked at each V_C in the *I–V* curve (Fig. 6*B*) and was calculated from the equation, $g_{Ca} = I_{Ca}/(V_C - E_{Ca})$, assuming that the I_{Ca}

is proportional to the driving force ($V_C - E_{Ca}$) and that the zero-current potential corresponds to the Ca^{2+} equilibrium potential (E_{Ca}). At a higher clamp potential of over +10 mV in Fig. 7*A*, g_{Ca} was further corrected to compensate for the steady-state inactivation of I_{Ca}, which was provided by the protocol similar to the one in Fig.

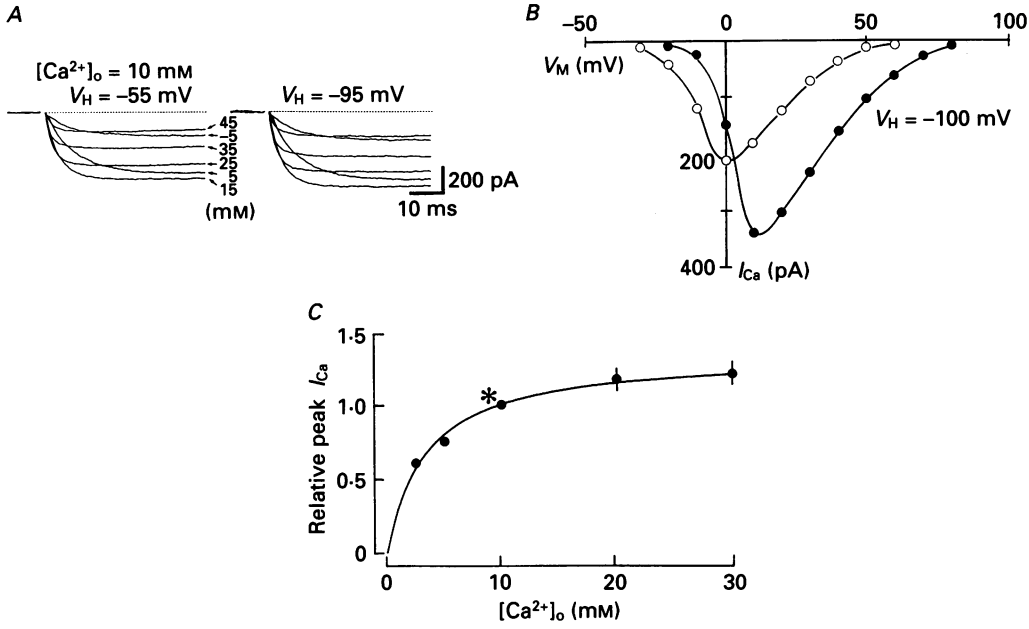

Fig. 6. Properties of the voltage-dependent Ca^{2+} current (I_{Ca}). *A*, I_{Ca} recorded from the same cell at V_H −55 and −95 mV. Depolarizing pulses to −5, +5, +15, +25, +35 and +45 mV from both V_H were applied. The $[Ca^{2+}]_o$ was 10 mV. The currents were corrected for leakage and transient capacitative currents after blocking I_{Ca} with 0·5 mM Cd^{2+}. *B*, *I–V* relationships for peak I_{Ca} recorded in the external solutions with 2·5 (○) or 10 mM Ca^{2+} (●). Data were obtained from the same cell at a V_H of −100 mV. The Ca^{2+} equilibrium potential (E_{Ca}) in the *I–V* relationship for I_{Ca} at 10 mM $[Ca^{2+}]_o$ was assumed to be +90 mV. *C*, relationship between peak amplitude of I_{Ca} and $[Ca^{2+}]_o$. The peak amplitude in the individual *I–V* relationships for I_{Ca} at various $[Ca^{2+}]_o$ was normalized to that (*) at 10 mM $[Ca^{2+}]_o$. A continuous curve was fitted by eqn (3) (see text). The data points are means ± S.E.M. ($n = 5$).

7*B*. Figure 7*A* shows that a threshold V_C for the I_{Ca} activation is −20 mV and that the full activation (the maximum g_{Ca}) is achieved at a V_C of +20 mV. The half-maximum activation V_C of 0·94 mV and the slope factor of −4·15 mV were obtained from a continuous curve fitted by the Bolzmann equation.

The steady-state inactivation of I_{Ca} was studied by the use of a double-pulse protocol (Fig. 7*B* inset). The $[Ca^{2+}]_o$ was 10 mM. The cell was depolarized by a conditioning prepulse of 300 ms or 1 s from a V_H of −100 mV, and then a 100 ms test pulse to +20 mV was applied after an interval of 1 ms. The currents elicited by the test pulse were normalized to that obtained in the absence of prepulse. To elucidate the dependence of I_{Ca} inactivation on intracellular Ca^{2+} accumulation, this study was carried out with internal solutions containing EGTA of two different concentrations (0·1 and 10 mM). Peak I_{Ca} decreased at prepulse potentials of −30 mV or more

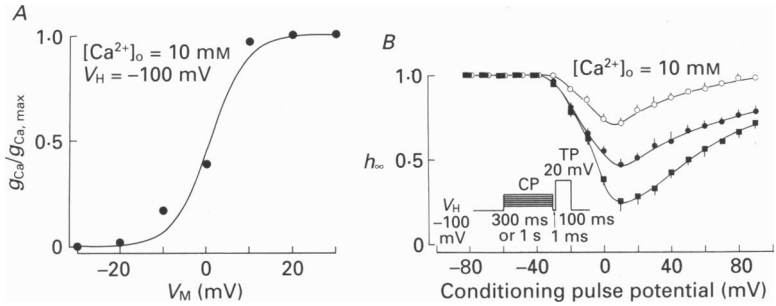

Fig. 7. Activation and inactivation of I_{Ca}. *A*, conductance–voltage relationship for I_{Ca}. The $[Ca^{2+}]_o$ was 10 mM. A continuous curve was fitted by the Boltzmann equation. *B*, steady-state inactivation (h_∞) curve for I_{Ca}. The $[Ca^{2+}]_o$ was 10 mM. The studies were carried out in internal solutions containing 0·1 and 10 mM EGTA. The conditioning prepulse (CP) durations in 10 mM EGTA; were 300 ms (○) and 1 s (●); and in 0·1 mM EGTA; 1 s (■). The pulse protocol is given in the text. All continuous were drawn by eye. The data points are means ± S.E.M. (n = 4–5).

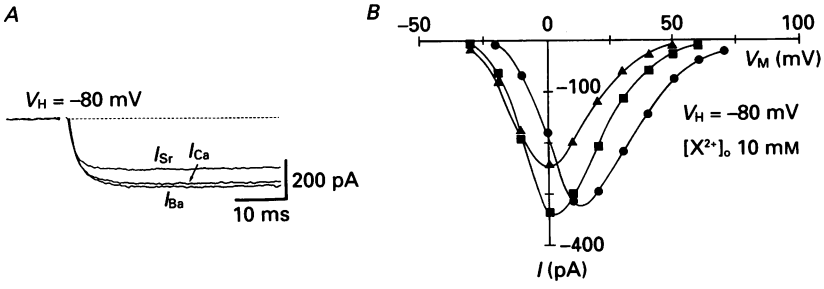

Fig. 8. Ionic selectivity of Ca^{2+} channels. *A*, maximum inward currents carried by Ca^{2+}, Ba^{2+} and Sr^{2+} in the same cell held at a V_H of −80 mV. Test potentials for I_{Ca}, I_{Ba} and I_{Sr} were +10, 0 and 0 mV, respectively. The currents were corrected by Cd^{2+} subtraction (see text). The concentration of the external divalent cation was 10 mM. *B*, representative *I–V* relationships for I_{Ca} (●), I_{Ba} (■) and I_{Sr} (▲) passing through Ca^{2+} channels. The data were obtained from the same cell as in *A*. V_H was −80 mV.

positive, reached its minimum value at a potential of +10 mV, and then increased at more positive potentials. In the cells perfused internally with 10 mM EGTA, the minimum values were about 70 and 45% when the prepulse duration was 300 ms and 1 s, respectively. In the cells perfused internally with 0·1 mM EGTA, the minimum value was about 25% at a prepulse duration of 1 s (Fig. 7*B*).

Ionic selectivity of Ca^{2+} channels was estimated from the maximum inward currents in individual *I–V* relationships, in which 10 mM Ca^{2+} in external solution was replaced with an equimolar Ba^{2+} or Sr^{2+}. The replacement of external Ca^{2+} with Ba^{2+} induced a little increase in the current amplitude, but the replacement with Sr^{2+} decreased it. However, the current kinetics was not affected by the replacement of Ca^{2+} with either Ba^{2+} or Sr^{2+} (Fig. 8*A*). Figure 8*B* shows *I–V* relationships for these divalent cation currents. Taking into account the different effects of these divalent cations on the membrane surface charge, we compared the maximum peak currents of individual *I–V* relationships in the presence of Ca^{2+}, Ba^{2+} and Sr^{2+}. The ratio of the

maximum peak value of Ca^{2+}, Ba^{2+} and Sr^{2+} currents was 1·00: 1·10±0·04: 0·75±0·02 (mean±S.E.M., $n = 8$).

Inhibitory effects of inorganic Ca^{2+} antagonists on I_{Ca} were studied. The currents were evoked by a 100 ms depolarization pulse to +20 mV from a V_H of −80 mV

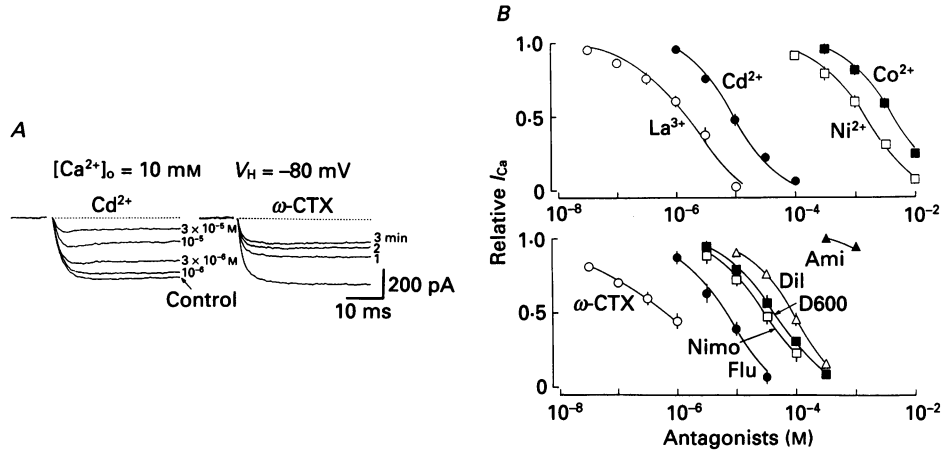

Fig. 9. Effects of inorganic and organic Ca^{2+} antagonists on I_{Ca}. *A*, effects of Cd^{2+} of various concentrations and 10^{-6} M ω-conotoxin (ω-CTX) on I_{Ca}. The currents were corrected by Cd^{2+} subtraction. Each blocker was applied to the same cell at a V_H of −80 mV, and test pulse was applied to 0 mV. *B*, concentration-dependent blockade of I_{Ca} by inorganic (upper panel) and organic lower panel) Ca^{2+} blockers. The $[Ca^{2+}]_o$ was 10 mM. The data points are means±S.E.M. ($n = 4$–6). All lines were drawn by eye. Flu, flunarizine; Nimo, nimodipine; Dil, diltiazem; Ami, amiloride.

every 30 s. Since the inhibition of I_{Ca} by polyvalent cations had no time dependence, the measurements were made after 30 s of adding inorganic Ca^{2+} blockers (Fig. 9*A* left panel). The polyvalent cations inhibited I_{Ca} in a concentration-dependent manner. The inhibitory sequence was in the order of $La^{3+} > Cd^{2+} \gg Ni^{2+} > Co^{2+}$. The IC_{50} values were $1{\cdot}5 \times 10^{-6}$ M for La^{3+}, 9×10^{-6} M for Cd^{2+}, $1{\cdot}5 \times 10^{-3}$ M for Ni^{2+} and 4×10^{-3} M for Co^{2+} (Fig. 9*B*, upper panel). The effects of these inorganic Ca^{2+} antagonists were completely reversible by washing out the antagonists. The inhibitory effects of organic Ca^{2+} antagonists on I_{Ca} were also examined. The effects of diltiazem (Dil), D600, nimodipine (Nimo) and amiloride (Ami) reached steady-state inhibition within 60 s of adding drugs whereas those of flunarizine (Flu) and ω-conotoxin (ω-CTX) developed more slowly (Fig. 9*A* right panel). Therefore, the steady-state inhibition to respective concentrations of organic Ca^{2+} antagonists was measured 3 min after adding all drugs. The inhibitory effects of organic Ca^{2+} antagonists were also concentration dependent. However, the inhibitory effect of ω-CTX did not develop beyond 10^{-6} M. Consequently, the maximum inhibition of ω-CTX on the I_{Ca} was 62·2±1·5% ($n = 6$) of control. The inhibitory sequence was ω-CTX ≫ flunarizine ≫ nimodipine > D600 > diltiazem ≫ amiloride. The values of IC_{50} were 8×10^{-6} M for flunarizine, 3×10^{-5} M for nimodipine, 4×10^{-5} M for D600 and 9×10^{-5} M for diltiazem (Fig. 9*B*, lower panel). The IC_{50} value of the ω-CTX-sensitive current component was $1{\cdot}1 \times 10^{-7}$ M. The inhibitory effects of amiloride,

diltiazem and D600 were completely reversible whereas those of nimodipine and flunarizine were incompletely recovered by washing out the antagonists. The effect of ω-conotoxin was recovered a little (10–15%) after 5 min of recovery.

Potassium current (I_K)

The voltage-dependent potassium current (I_K) was separated by the use of an external E_3 solution with 5 mM K^+ and an internal I_3 solution with 120 mM K^+ (Table

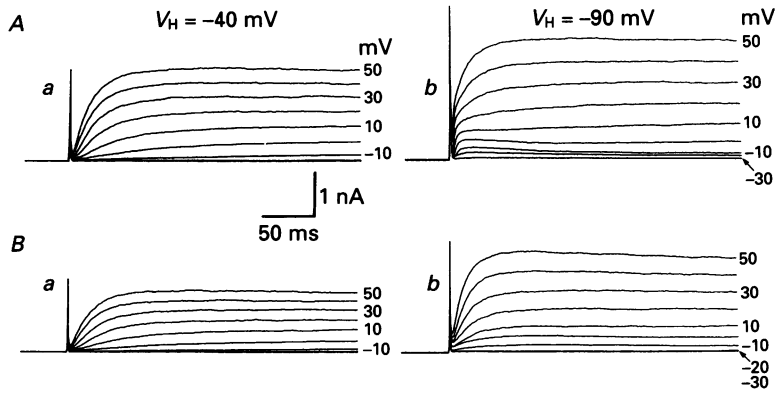

Fig. 10. Effects of two different V_H on the voltage-dependent I_K. Currents were evoked from V_H −40 or −90 mV. Test pulses to potentials between −30 and +50 mV were applied from both V_H. No corrections were made for leakage or capacitative currents. *A* and *B* were obtained from a 'type A' cell and a 'type B' cell, respectively (see text).

1). The I_{Na} was completely eliminated by both the substitution of external Na^+ with NMG^+ and the addition of 3×10^{-6} M TTX to the external solution. The I_{Ca} was blocked by adding 0·5 mM Cd^{2+} to the external solution. Under these experimental conditions, three types of I_K were observed depending on the V_H used: a delayed outward current (I_{KD}), a transient outward current (I_A), and an inwardly rectifying current (the anomalous rectifier). Since the anomalous rectifier has been well characterized in the same paratracheal ganglion cells (Allen & Burnstock, 1990a), we will not discuss this current further.

In the study of I_K, two cells types were observed. One cell type exhibited a detectable I_A ($n = 44$) whereas the other cell type exhibited no detectable I_A ($n = 19$). We termed the former 'type A' cells and the latter 'type B' cells.

Figure 10*Aa* and *Ab* shows I_K recorded from a 'type A' cell at V_H of −40 and −90 mV, respectively. From a V_H of −40 mV, depolarizing pulses to −10 mV or more positive potentials elicited large outward K^+ currents. These currents activated slowly, showed little inactivation and were sustained during the depolarizing pulse, in a manner corresponding to I_{KD} (Fig. 10*Aa*). Depolarizing steps to −20 mV or more positive potentials from a V_H of −90 mV elicited not only I_{KD} but also small transient outward currents corresponding to I_A, and the I_{KD} overlapped on I_A (Fig. 10*Ab*). The I_A was not affected by the removal of extracellular Ca^{2+} from these neurones ($n = 13$). Figure 10*Ba* and *Bb* shows the currents recorded from a 'type B' cell at V_H of −40 and −90 mV, respectively. But in the case of the 'type A' cell, although I_{KD} was observed, there was no detectable I_A even at a V_H of −90 mV.

The I–V relationships for two types of I_K were studied in 'type A' cells before and during application of 3 mM 4-aminopyridine (4-AP). A 500 ms test pulse was applied to a series of test potentials from a V_H of −100 mV. Application of 4-AP suppressed a transient current component of K^+ current, I_A (Fig. 11*A b*). Computer subtraction

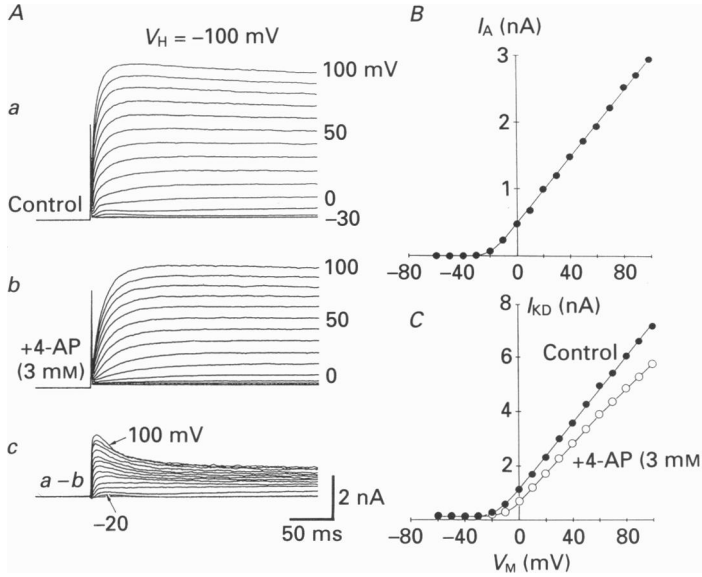

Fig. 11. Effects of 4-aminopyridine (4-AP) on I_K in 'type A' cell. *A*, outward currents evoked by test pulses from a V_H of −100 mV before (*a*) and during (*b*) application of 3 mM 4-AP. *A c* shows the currents blocked by 4-AP, obtained by computer subtraction of records in *b* from those in *a*. The step pulses of 10 mV increments from −60 to +100 mV were applied. *B*, *I–V* relationships of I_A, measured as the peak current in *A c*. *C*, *I–V* relationships of I_{KD} measured at 250 ms after the onset of the test pulse before and during 4-AP application.

of outward currents before and during 4-AP applications shows the I_A blocked by 4-AP (Fig. 11*A c*). The time course and peak amplitude of 4-AP-sensitive I_A were dependent on the test potential. This I_A developed from a threshold potential near −20 mV (Fig. 11*B*) and was characterized by fast activation and inactivation. As shown in Fig. 11*C*, 3 mM 4-AP also partially blocked the I_{KD} by decreasing the conductance, which is indicated by the different slopes of the *I–V* relationships obtained before and during 4-AP application.

Steady-state inactivation of I_{KD} was studied in the 'type B' cells by the use of a double-pulse protocol (Fig. 12*A*, inset). A 10 s conditioning prepulse was applied to various potentials from a V_H of −90 mV. Then a 1 s test pulse was applied to +50 mV after an interval of 1 ms. The current elicited by the test pulse was normalized to that obtained in the absence of prepulse. A continuous line in Fig. 12*A* was well fitted by the Boltzmann equation. The I_{KD} became inactivated at a potential more positive than −60 mV. The half-inactivation potential and the slope factor were $-37 \pm 2{\cdot}8$ and $6{\cdot}0 \pm 0{\cdot}3$ mV, respectively.

The effect of tetraethylammonium chloride (TEA-Cl) on I_{KD} was examined. Before

TEA application, the *I–V* relationship for I_{KD} was determined at a V_H of −40 mV. Then the second *I–V* relationship for I_{KD} was determined during the 10 mM TEA application. The I_{KD} decreased within 5–10 s of TEA application, and the effect remained stable until the removal of the drug. The effect of TEA was completely

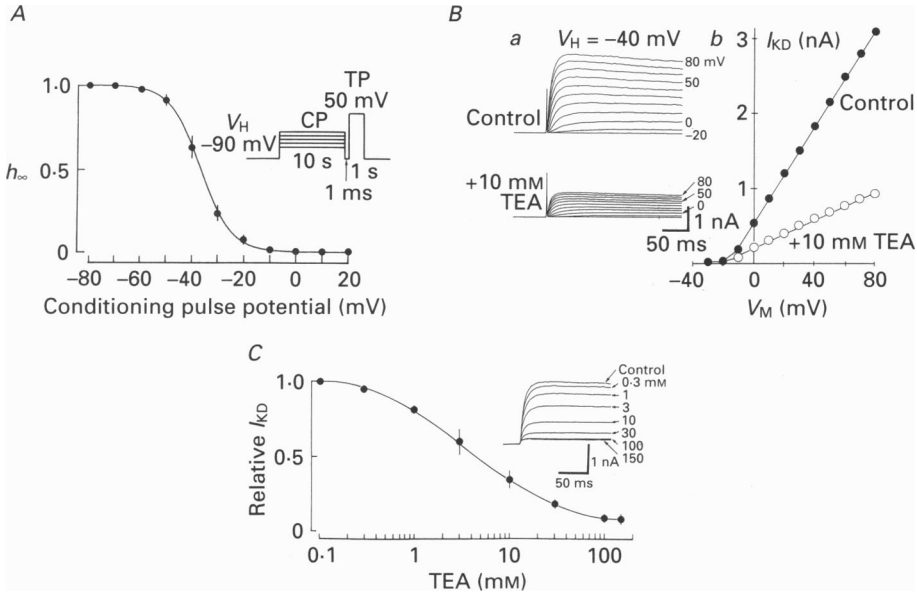

Fig. 12. Properties of I_{KD}. *A*, steady-state inactivation (h_∞) curve for I_{KD} studied in 'type B' cells. The pulse protocol is shown in the inset. A continuous line was fitted by the Boltzmann equation. The data points are means ± S.E.M. (n = 4–5). *B*, effect of TEA on I_{KD}. *a*, outward currents evoked by step pulses from a V_H of −40 mV before (upper traces) and during 10 mM TEA application (lower traces). The traces were obtained from one cell. *b*, *I–V* relationships of I_{KD} measured 100 ms after the onset of the test pulse before and during 10 mM TEA application. The test pulses were applied to potentials between −30 and +80 mV from a V_H of −40 mV. *C*, concentration-dependent inhibition of I_{KD} by TEA. The current was evoked by a test pulse to +60 mV from a V_H of −40 mV. The inset shows the outward currents before and during TEA application of various concentrations. The leakage current was removed by computer subtraction of the response by a 5 mV negative voltage step. The data points are means ± S.E.M. (n = 4–5). A continuous line was drawn by eye.

reversed by washing out the drug. TEA did not affect the threshold of I_{KD}, but clearly diminished the conductance, as is indicated by the different slopes of the *I–V* relationships obtained before and during TEA application (Fig. 12*Bb*). TEA suppressed the I_{KD} in a concentration-dependent manner (Fig. 12*C*). The threshold concentration of the TEA depression of I_{KD} was 0·3 mM and IC_{50} was 4·4 mM. The I_{KD} was not completely abolished even by 150 mM of TEA application.

Voltage-dependent inactivation of I_A was studied in the 'type A' cells, using the following protocol. I_A was recorded at a V_H of −10 mV following a 100 ms step to a series of prepulse potentials more negative than −20 mV. As shown in Fig. 13*B*, I_A was activated when the prepulse potential was more negative than −40 mV. The current was fully activated by a prepulse potential of −100 mV. The half-

inactivation potential was −70 mV. To study the recovery from the complete inactivation of I_A, various durations of a negative pulse to −100 mV from a V_H of −10 mV was applied. The I_A recovered with the prolongation of the hyperpolarized pulse duration. The conditioning pulse caused it to recover to 50% of the control

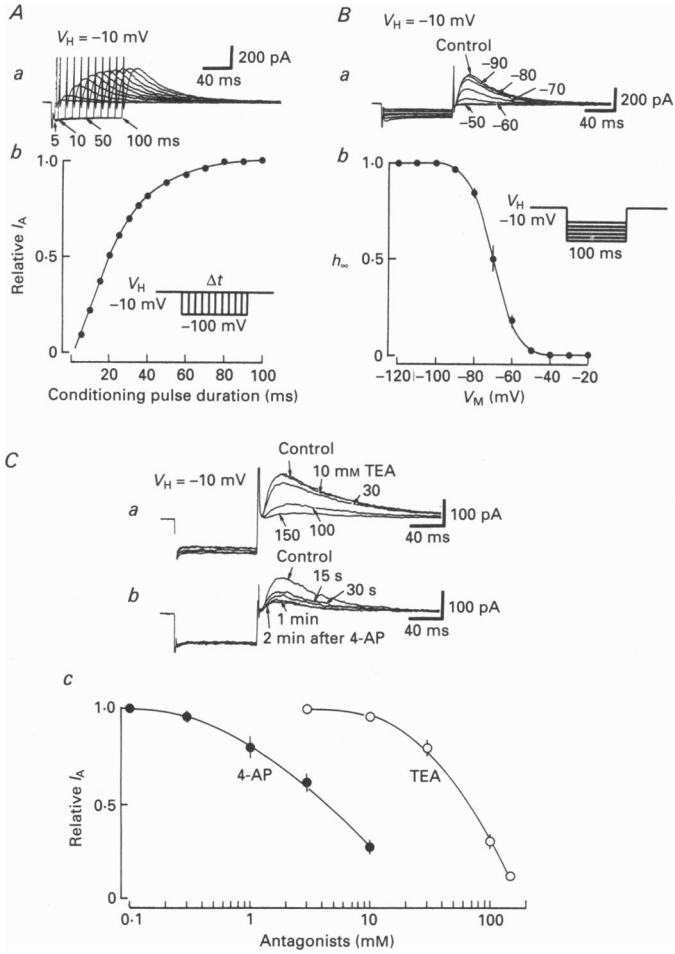

Fig. 13. Properties of I_A. *A*, recovery of I_A from inactivation. The pulse protocol in the inset shows that the membrane potential was stepped from −10 to −100 mV for time periods between 5 and 100 ms. Normalized data are plotted as a function of the pulse interval. The line was drawn by eye. *B*, steady-state inactivation (h_∞) curve of I_A constructed from the pulse protocol shown in the inset. Outward currents show the transient current responses on the return of the membrane potential to a V_H of −10 mV after a series of voltage negative steps. The h_∞ was maximal at −100 mV. A continuous line was fitted by the Boltzmann equation. The data points are means ± S.E.M. (n = 4–5). *C*, effects of TEA of various concentrations (*a*) and 10 mM 4-AP (*b*) on reactivated I_A. Outward currents were recorded at a V_H of −10 mV following a 100 ms negative pulse to −100 mV. *C*, concentration–inhibition curves of TEA and 4-AP on I_A. The data points are means ± S.E.M. (n = 4–6). The lines were drawn by eye.

value after about 20 ms. Recovery from inactivation was essentially complete after holding the cell at −100 mV for 80–100 ms (Fig. 13*A*). As already noted, in this preparation, I_A and I_{KD} could not be completely separated from each other using

their differences in voltage dependence, as previously described by Connor & Stevens (1971). Hence, the effects of K^+ channel blockers on I_A were studied by the use of reactivated I_A. The current was recorded at a V_H of -10 mV following a 100 ms negative pulse to -100 mV. The inhibitory action of TEA had no time dependence, so the measurements were made 30 s after adding the blocker (Fig. 13*Ca*). The inhibitory action of 4-AP developed more slowly, so the inhibition to respective concentrations of 4-AP was measured 2 min after adding the blocker (Fig. 13*Cb*). The effect of TEA was completely recovered by washing out the blocker while that of 4-AP was partially recovered. I_A was inhibited by both TEA and 4-AP in a concentration-dependent manner, though I_A was more sensitive to 4-AP than TEA, as was also previously described in another preparation (Rudy, 1988). The threshold concentrations of 4-AP and TEA depressing I_A were 0·3 and 10 mM, and IC_{50} values for 4-AP and TEA were 4·3 and 70 mM, respectively (Fig. 13*Cc*).

DISCUSSION

Sodium current (I_{Na})

The voltage-dependent Na^+ channels have been most thoroughly studied in nerve and muscle cells, and TTX-resistant I_{Na} has been described with regard to cardiac cells (Cohen, Bean, Colatsky & Tsien, 1981), neurones (Gallego, 1983; Bossu & Feltz, 1984) and skeletal muscle fibres (Weiss & Horn, 1986). It has also been reported that trypsin treatment reduced the sensitivity of Na^+ channels to TTX (Lee, Akaike & Brown, 1977). However, there was no TTX-resistant component of I_{Na} in this preparation, regardless of the trypsin treatment in the cell dissociation procedure (see Methods). Hence, the voltage-dependent I_{Na} in this preparation is highly TTX sensitive.

The Na^+ channel was activated at potentials more positive than -50 mV in this preparation. This activation range of the Na^+ channel was similar to those in rat dorsal root ganglion neurones (Kostyuk, Veselovsky & Tsyndrenko, 1981), rat nodose ganglion cells (Ikeda, Schofield & Weight, 1986) and rat papillary muscles (Antoni, Bocker & Eickhorn, 1988).

From analyses of the steady-state inactivation and inactivation kinetics of I_{Na} in this preparation, we have concluded as follows: (1) the time course of inactivation is not well represented by a single exponential process; (2) the time course of I_{Na} decay is second order; (3) the time course of recovery of I_{Na} from inactivation is not well represented by a single exponential process. Taken together, the results are consistent with the presence of at least two inactivated states for the voltage-dependent Na^+ channels, as was the case with cardiac cells (Brown, Lee & Powell, 1981; Cachelin, Depeyer, Kokubun & Reuter, 1983; Follmer, Ten Eick & Yeh, 1987; Antoni *et al.* 1988) and in nerve cells (Chiu, 1977; Meves, 1978).

The results of our analysis of the action of scorpion toxin may further substantiate the case for the presence of two inactivated states in the Na^+ channel. In this study, scorpion toxin increased in a concentration-dependent manner both the time constant of the slow component and its fractional contribution to the total current. On the other hand, the fractional contribution of the fast component was reduced without changing its time constant. From these results it is possible to propose that toxin transforms the channel state forming the fast exponential component into that

forming the slow component of which the time constant is profoundly increased by the toxin. An increase in the time constant of the slow component may reflect the changes in channel kinetics, such as in increase in open time, a decreased in closed time or both.

Calcium currents (I_{Ca})

The properties of the Ca^{2+} channels in this preparation were similar to those in sympathetic neurones of the chick (Marchetti, Carbone & Lux, 1986), rat (Wanke, Ferroni Malgaroli, Ambrosini, Pozzan & Meldolesi, 1987) and frog (Jones & Marks, 1989). They have the same threshold for activation (the range of -40 to -30 mV) and maximum values in I–V relationships (the range of 0 to $+10$ mV) at 2–5 mM $[Ca^{2+}]_o$. Additionally, the rat paratracheal neurones had no 'low-voltage-activated' ('T-type') Ca^{2+} channels.

From analysis of the steady-state inactivation of I_{Ca} in this preparation, we obtained the following findings: (1) the extent of inactivation is maximum for depolarizations yielding maximal I_{Ca}; (2) the extent of inactivation is modified by the duration of the depolarizing prepulse accompanying Ca^{2+} influx; (3) the extent of inactivation is modified by intracellular concentration of EGTA. These results suggest that the inactivation of I_{Ca} largely reflects Ca^{2+}-dependent inactivation in this preparation as well as in invertebrate neurones (Plant, Standen & Ward, 1983), rat sympathetic neurones (Adams & Galvan, 1986) and frog sensory neurones (Akaike, Tsuda & Oyama, 1988).

The pharmacological properties of I_{Ca} in this preparation were very similar to those of 'high-voltage-activated' ('L-type') I_{Ca} described in reference to many other neurones (for review, see Swandulla, Carbone & Lux, 1991) e.g. (1) Cd^{2+} strongly reduced the current at low concentrations ($IC_{50} = 9 \times 10^{-6}$ M); (2) ω-conotoxin also suppressed the current at micromolar concentrations; (3) the current was not reduced by micromolar concentrations of Ni^{2+}. The current was insensitive to amiloride.

Potassium currents (I_K)

The threshold for activation of I_{KD} in this preparation was more depolarized than that of 'delayed rectifier' in other vertebrate neurones, which is typically between -50 and -40 mV (for commentary, see Rudy, 1988). However, the I_{KD} of rat paratracheal neurones inactivated slowly ($\tau > 1$ s), and it was sensitive to TEA ($IC_{50} = 4{\cdot}4$ mM), as well as 'delayed rectifier' (Rudy, 1988).

Although the threshold for activation of I_A in this preparation was more depolarized than that of 'A-current' noted in other neurones (which are typically near -60 mV), the fast activation and the sensitivity to 4-AP indicate that this current corresponds to the A-current. Additionally, this current quickly inactivated, and steady-state inactivation was complete at near resting potential as well as A-current (Rudy, 1988). The amplitude and the time course of I_A were dependent on $[Ca^{2+}]_o$ in invertebrate neurones (Thompson, 1977), in hippocampal neurones (Gustafsson, Galvan, Grafe & Wigstrom, 1982), in rat sympathetic neurones (Galvan & Sedlmeir, 1984) and in rat supraoptic neurones (Bourque, 1988). In this study,

however, the I_A in all 'type A' cells tested was unaffected by removal of extracellular Ca^{2+}, as was also previously reported in the case of rat sympathetic neurones (Belluzzi, Sacchi & Wanke, 1985).

The tension of airway smooth muscle in many species is controlled by excitatory neural inputs transmitted via the vagus nerves. The paratracheal ganglion cells are the last relay stations for the neural inputs to the airway smooth muscle. Therefore, information concerning the properties of their transmembrane ionic currents and further studies about modulation of these currents by both neurotransmitters and neuropeptides will enhance our understanding of the parasympathetic control in airway smooth muscle tone.

The authors thank Y. Ito for helpful advice and B. Bell for revising the manuscript. This investigation was supported by Grant-in-Aid for Scientific Research (Nos. 02557005 and 03304026 to N.A.) from The Ministry of Education, Science and Culture, Japan.

REFERENCES

ADAMS, P. R. & GALVAN, M. (1986). Voltage-dependent currents in vertebrate neurones and their role in membrane excitability. *Advances in Neurology* **44**, 137–170.

AIBARA, K. & AKAIKE, N. (1991). Acetylcholine-activated ionic currents in isolated paratracheal ganglion cells of the rat. *Brain Research* **558**, 20–26.

AKAIKE, N., SHIRASAKI, T. & YAKUSHIJI, T. (1991). Quinolones and fenbufen interact with $GABA_A$ receptor in dissociated hippocampal cells of rat. *Journal of Neurophysiology* **66**, 497–504.

AKAIKE, N., TSUDA, Y. & OYAMA, Y. (1988). Separation of current- and voltage-dependent inactivation of calcium current in frog sensory neuron. *Neuroscience Letters* **84**, 46–50.

ALLEN, T. G. J. & BURNSTOCK, G. (1990*a*). A voltage-clamp study of the electrophysiological characteristics of the intramural neurones of the rat trachea. *Journal of Physiology* **423**, 593–614.

ALLEN, T. G. J. & BURNSTOCK, G. (1990*b*). $GABA_A$ receptor-mediated increase in membrane chloride conductance in rat paratracheal neurones. *British Journal of Pharmacology* **100**, 261–268.

ANTONI, H., BOCKER, D. & EICKHORN, R. (1988). Sodium current kinetics in intact rat papillary muscles: measurements with the loose-patch-clamp technique. *Journal of Physiology* **406**, 199–213.

BELLUZZI, O., SACCHI, O. & WANKE, E. (1985). A transient outward current in the rat sympathetic neurone studied under voltage-clamp conditions. *Journal of Physiology* **358**, 91–108.

BENOIT, E. & DUBOIS, J. (1987). Properties of maintained sodium current induced by a toxin from *Androctonus* scorpion in frog node of Ranvier. *Journal of Physiology* **383**, 93–114.

BOSSU, J. L. & FELTZ, A. (1984). Patch-clamp study of the tetrodotoxin-resistant sodium current in group C sensory neurones. *Neuroscience Letters* **51**, 241–246.

BOURQUE, C. W. (1988). Transient calcium-dependent potassium current in magnocellular neurosecretory cells of the rat supraoptic nucleus. *Journal of Physiology* **397**, 331–347.

BROWN, A. M., LEE, K. S. & POWELL, T. (1981). Sodium current in single rat heart muscle cells. *Journal of Physiology* **318**, 479–500.

BURNSTOCK G., ALLEN, T. G. J. & HASSALL, C. J. S. (1987). The electrophysiologic and neurochemical properties of paratracheal neurones *in situ* and in dissociated cell culture. *American Review of Respiratory Disease* **136**, S23–26.

CACHELIN, A. B., DEPEYER, J. E. & KOKUBUN, S. & REUTER, H. (1983). Sodium channels in cultured cardiac cells. *Journal of Physiology* **340**, 389–401.

CARBONE, E. & LUX, H. D. (1987). Kinetics and selectivity of a low voltage-activated calcium current in chick and rat sensory neurones. *Journal of Physiology* **386**, 547–570.

CHIU, S. Y. (1977). Inactivation of sodium channels: second order kinetics in myelinated nerve. *Journal of Physiology* **273**, 573–596.

COBURN, R. F. (1987). Peripheral airway ganglia. *Annual Review of Physiology* **49**, 573–582.

COHEN, C. J., BEAN, B. P., COLATSKY, T. J. & TSIEN, R. W. (1981). Tetrodotoxin block of sodium channels in rabbit Purkinje fibers. *Journal of General Physiology* **78**, 383–411.

CONNOR, J. A. & STEVENS, C. F. (1971). Voltage clamp studies of a transient outward membrane current in gastropod neural somata. *Journal of Physiology* **213**, 21–30.

FISHER, A. W. (1964). The intrinsic innervation of the trachea. *Journal of Anatomy* **98**, 117–124.

FOLLMER, C. H., TEN EICK, R. E. & YEH, J. Z. (1987). Sodium current kinetics in cat atrial myocytes. *Journal of Physiology* **384**, 169–197.

GALLEGO, R. (1983). The ionic basis of action potentials in petrosal ganglion cells of the cat. *Journal of Physiology* **342**, 591–602.

GALVAN, M. & SEDLMEIR, C. (1984). Outward currents in voltage-clamped rat sympathetic neurones. *Journal of Physiology* **356**, 115–133.

GONOI, T., HILLE, B. & CATTERALL, W. A. (1984). Voltage clamp analysis of sodium channels in normal and scorpion toxin-resistant neuroblastoma cells. *Journal of Neuroscience* **4**, 2836–2842.

GUSTAFSSON, B., GALVAN M., GRAFE, P. & WIGSTROM, H. (1982). A transient outward current in a mammalian central neurone blocked by 4-aminopyridine. *Nature* **299**, 252–254.

HAMILL, O. P., MARTY, A., NEHER, E., SAKMANN, B. & SIGWORTH, F. J. (1981). Improved patch-clamp techniques for high resolution current recording from cells and cell-free membrane patches. *Pflügers Archiv* **391**, 85–100.

HONJIN, R. (1954). On the ganglia and nerves of the lower respiratory tract of the mouse. *Journal of Morphology* **95**, 263–288.

IKEDA, S. R., SCHOFIELD, G. G. & WEIGHT, F. F. (1986). Na^+ and Ca^{2+} currents of acutely isolated adult rat nodose ganglion cells. *Journal of Neurophysiology* **55**, 527–539.

JONES, S. W. & MARKS, T. N. (1989). Calcium currents in bullfrog sympathetic neurons. I. Activation kinetics and pharmacology. *Journal of General Physiology* **94**, 151–167.

KANEDA, M., OYAMA, T., IKEMOTO, T. & AKAIKE, N. (1989*a*). Blockade of the voltage-dependent sodium current in isolated rat hippocampal neurons by tetrodotoxin and lidocaine. *Brain Research* **484**, 348–351.

KANEDA, M., OYAMA, Y., IKEMOTO, Y. & AKAIKE, N. (1989*b*). Scorpion toxin prolongs an inactivation phase of the voltage-dependent sodium current in rat isolated single hippocampal neurons. *Brain Research* **487**, 192–195.

KOSTYUK, P. G. (1984). Intracellular perfusion of nerve cells and its effect on membrane currents. *Physiological Reviews* **64**, 435–454.

KOSTYUK, P. G., VESELOVSKY, N. S. & TSYNDRENKO, A. Y. (1981). Ionic currents in the somatic membrane of rat dorsal root ganglion neurons. I. Sodium currents. *Neuroscience* **6**, 2423–2430.

LEE, K. S., AKAIKE, N. & BROWN, A. M. (1977). Trypsin inhibits the action of tetrodotoxin on neurones. *Nature* **265**, 751–753.

MARCHETTI, C., CARBONE, E. & LUX, H. D. (1986). Effects of dopamine and noradrenaline on Ca channels of cultured sensory and sympathetic neurons of chick. *Pflügers Archiv* **406**, 104–111.

MEVES, H. (1978). Inactivation of sodium permeability in squid giant nerve fibers. *Progress in Biophysics and Molecular Biology* **33**, 207–230.

NOWYCKY, M. C., FOX, A. P. & TSIEN, R. W. (1985). Three types of neuronal calcium channel with different calcium agonist sensitivity. *Nature* **316**, 440–443.

PLANT, A., STANDEN, N. B. & WARD, T. A. (1983). The effects of injection of calcium ions and calcium chelators on calcium channel inactivation in *Helix* neurones. *Journal of Physiology* **321**, 273–285.

RUDY, B. (1988). Diversity and ubiquity of K channels. *Neuroscience* **25**, 729–749.

SWANDULLA, D., CARBONE, E. & LUX, H. D. (1991). Do calcium channel classifications account for neuronal calcium channel diversity? *Trends in Neurosciences* **14**, 46–51.

THOMPSON, S. H. (1977). Three pharmacologically distinct potassium channels in molluscan neurones. *Journal of Physiology* **265**, 465–488.

WANKE, E., FERRONI, A., MALGAROLI, A., AMBROSINI, A., POZZAN, T. & MELDOLESI, J. (1987). Activation of a muscarinic receptor selectively inhibits a rapidly inactivated Ca^{2+} current in rat sympathetic neurons. *Proceedings of the National Academy of Sciences of the USA* **84**, 4313–4317.

WEISS, R. E. & HORN, R. (1986). Functional differences between two classes of sodium channels in developing rat skeletal muscle. *Science* **233**, 361–364.

YASUI, S. & AKAIKE, N. (1986). Saturation, binding, selectivity and activation energy profile associated with the calcium channel. *Kumamoto Medical Journal* **39**, 105–128.